

Jensen's force and the statistical mechanics of cortical asynchronous states

Victor Buendía^{1,2,3}, Pablo Villegas¹, Serena di Santo⁴, Alessandro Vezzani^{2,5}, Raffaella Burioni^{2,3}, and Miguel A. Muñoz^{1,2}

¹Departamento de Electromagnetismo y Física de la Materia e Instituto Carlos I de Física Teórica y Computacional. Universidad de Granada. E-18071, Granada, Spain

²Dipartimento di Matematica, Fisica e Informatica, Università di Parma, via G.P. Usberti, 7/A - 43124, Parma, Italy

³INFN, Gruppo Collegato di Parma, via G.P. Usberti, 7/A - 43124, Parma, Italy

⁴Scuola Internazionale Superiore di Studi Avanzati, via Bonomea, 265 - 34136 Trieste, Italy.

⁵IMEM-CNR, Parco Area delle Scienze 37/A - 43124 Parma, Italy

Abstract

The cortex exhibits self-sustained highly-irregular activity even under resting conditions, whose origin and function need to be fully understood. It is believed that this can be described as an "asynchronous state" stemming from the balance between excitation and inhibition, with important consequences for information-processing, though a competing hypothesis claims it stems from critical dynamics. By analyzing a parsimonious neural-network model with excitatory and inhibitory interactions, we elucidate a noise-induced mechanism called "Jensen's force" responsible for the emergence of a novel phase of arbitrarily-low but self-sustained activity, which reproduces all the experimental features of asynchronous states. The simplicity of our framework allows for a deep understanding of asynchronous states from a broad statistical-mechanics perspective and of the phase transitions to other standard phases it exhibits, opening the door to reconcile, asynchronous-state and critical-state hypotheses. We argue that Jensen's forces are measurable experimentally and might be relevant in contexts beyond neuroscience.

Networks of excitatory units –in which some form of "activity" propagates between connected nodes– are successfully used as abstract representations of propagation phenomena as varied as epidemics, computer viruses, or memes in social networks [1]. Such dynamical processes can be either in an *active* phase in which activity reverberates indefinitely through the network or in a *quiescent* phase where activity eventually ceases; in some cases of interest they lie at the very edge of the quiescent/active phase transition [2, 3, 4].

Some systems of utmost biological relevance cannot be, however, modeled as networks of purely excitatory units. Nodes that inhibit (or repress) further activations are essential components of neuronal circuits in the cortex [5], as well as of gene-regulatory, signaling, and metabolic networks [6, 7]. Indeed, an essential feature of cortical networks is that they are composed of both excitatory and inhibitory neurons; synaptic excitation occurs always in concomitance with synaptic inhibition. What is the function of such a co-occurrence of excitation and inhibition? or, quoting a recent review article on the subject, "why should the cortex simultaneously push on the accelerator and on the brake?" [8].

Generally speaking, inhibition entails much richer sets of dynamical patterns including oscillations [9, 10] and counterintuitive phenomena. For example, in a nice and intriguing paper that triggered our curiosity, it was argued that inhibition induces "ceaseless" activity in excitatory/inhibitory (E/I) networks [11]. More in general, inhibition helps solving a fundamental

problem in neuroscience, namely, that of the dynamic range, defined as follows. Each neuron in the cortex is connected to many others, but individual synapses are relatively weak, so that each single neuron needs to integrate inputs from many others to become active; this leads to an explosive, all-or-none type of recruitment in populations of purely excitatory neurons, i.e. to a discontinuous phase transition between a quiescent and an active phase [8]. In other words, the network is either quiescent or almost saturated. This would severely constrain the set of possible network states, hindering the network capacity to produce diverse responses to differing inputs. This picture changes dramatically in the cortex, where the presence of inhibition has been empirically observed to allow for much larger dynamic ranges owing to a progressive (smoother) recruitment of neuronal populations [12, 13]. This is consistent with the well-known empirical fact that neurons in the cerebral cortex remain slightly active even in the absence of stimuli [14, 15, 16]. In such a state of low self-sustained activity neurons fire in a steady but highly-irregular fashion at a very low rate and with little correlations among them. This is the so-called *asynchronous state*, which has been argued to play an essential role for diverse computational tasks [17, 18, 19, 20].

It has become widely accepted that such an asynchronous state of low spontaneous activity emerges from the interplay between excitation and inhibition. Models of *balanced* E/I networks, in which excitatory and inhibitory inputs largely compensate each other, constitute –as it was first theoretically proposed [21, 22, 23, 24, 25] and then experimentally confirmed [26, 27, 28, 29, 30]– the basis to rationalize asynchronous states. Indeed, balanced E/I networks are nowadays considered as a sort of “standard model” of cortical dynamics [31].

In spite of solid theoretical and experimental advances, a full understanding of the phases of E/I networks remains elusive. For instance, it is still not clear if simple mathematical models can sustain highly-irregular low-activity phases even in the complete absence of external inputs from other brain regions. Indeed, many existing approaches to the asynchronous state assume that it requires of external inputs from other brain regions to be maintained [32], while some others rely on endogenously firing neurons –i.e. firing even without inputs– for the same purpose (see e.g. [33]). Furthermore, it is not clear from modelling approaches whether asynchronous states can have very low (rather than high or moderate) levels of activity [32, 34, 35].

All these problems can be summarized –from a broader Statistical Mechanics perspective– saying that it is not well-understood whether the asynchronous state constitutes an actual physical phase of self-sustained activity different from the standard quiescent and active ones. It is not clear either if novel non-standard types of phase transitions emerge at its boundaries. Such possible phase transitions might have important consequences for shedding light in to the so-called “criticality hypothesis”. This states that the cortex might operate close to the edge of a phase transition to optimize its performance; thus, it is essential to first understand what the possible phases and phase transitions are.

Here, we analyze the simplest possible network model including excitation and inhibition in an attempt to create a parsimonious model –understood as the simplest possible yet not-trivial model– of E/I networks [11]. We show, by employing a combination of theoretical and computational analyses, that the introduction of inhibitory interactions into purely excitatory networks leads to a self-sustained low-activity phase intermediate between conventional quiescent and active phases. Remarkably, the novel phase stems from a noise-induced mechanism that we call “Jensen’s force” (or “Jensen’s drift”) –for its relationship with Jensen’s inequality in probability theory– and that occurs owing to the combined effect of inhibition and network sparsity. The low-activity intermediate phase shares all its fundamental properties with asynchronous states and thus, as we argue, our model constitutes the simplest possible statistical-mechanics representation of asynchronous endogenous cortical activity. Moreover, continuous (critical) phase transitions –separating the novel intermediate phase from the quiescent and active phases, respectively– are elucidated, with possible important consequences to shed light on the criticality hypothesis [36, 4, 37], and to make an attempt to reconcile the asynchronous-state and

criticality hypotheses, putting them together within a unified framework. Finally, we propose that the elucidated Jensen’s force might be relevant in other contexts such as e.g. gene regulatory networks.

1 Models and Results

1.1 Minimal model

The simplest approach to capture the basic elements of E/I networks are two-state (binary) neuron models [21, 19], such as the one proposed by Larremore *et al.* [11]. The simplified version that we consider here consists of a random-regular directed network with N nodes and K links [38]. A fraction α of the nodes (typically $\alpha = 0.2$ to mimic empirical observations in the cortex [39, 30]) are *inhibitory* (negative interactions) and the rest are excitatory (positive interactions). More specifically, the network is *hyper-regular*, meaning that not only all nodes have the same inbound and outbound connectivity $k = K/N$, but also that each of them receives exactly αk inhibitory inbound links and $(1 - \alpha)k$ of excitatory ones (see Fig.1 and Methods).

At any given (discrete) time t the state of a single node, i , can be either active, $s_i(t) = 1$, or inactive $s_i(t) = 0$. The dynamics is such that each node i integrates the (weighted) activity of its k neighbors as sketched in Fig.1. At time $t + 1$, s_i becomes active (resp. inactive) with probability \mathcal{P}_i (resp. $1 - \mathcal{P}_i$) given by

$$\mathcal{P}_i \equiv f\left(\Lambda_i = \frac{\gamma}{k} \sum_j \omega_{ij} s_j(t)\right) = \begin{cases} 0 & \Lambda_i < 0 \\ \Lambda_i & 0 \leq \Lambda_i \leq 1 \\ 1 & \Lambda_i > 1 \end{cases} \quad (1)$$

where f is a transfer function of the input Λ_i , j runs over the set of (k) nodes pointing to node i , w_{ij} is the weight of the connection from node j to node i ($w_{ij} = \pm 1$, for simplicity), and γ is the overall coupling-strength that acts as a control parameter.

The model is kept purposely simple in an attempt to reveal the basic mechanisms of its collective behavior; more complex network architectures, transfer functions, and other realistic ingredients are implemented *a posteriori* to verify the robustness of the results.

1.2 Mean-field approach: massively connected networks:

We start considering the case of a fully connected network. Let E and I be the total number of excitatory and inhibitory active nodes, respectively, at a given time. These evolve stochastically according to a Master equation (as described in Methods), from which –performing a $1/N$ expansion– one readily obtains the following deterministic equations: $\dot{e} = (1 - \alpha) \langle f(\Lambda) \rangle - e$ and $\dot{i} = \alpha \langle f(\Lambda) \rangle - i$ –where the dot stands for time derivative– for $e = E/N$ and $i = I/N$, respectively. It follows that, in the steady state, excitation and inhibition are proportional to each other: $e/(1 - \alpha) = i/\alpha$, i.e. they become spontaneously balanced in a dynamical way. Moreover, the overall activity density, $s = e + i$, obeys

$$\dot{s} = \langle f(\Lambda) \rangle - s, \quad (2)$$

while the difference $q = e - i$ is simply proportional to s in the stationary state: $q = (1 - 2\alpha)s$. In the large network-size limit (i.e. $N \rightarrow \infty$), fluctuations in the input of each node are negligible. In such a limit, all nodes receive the same input, and thus the mean-field approach, in which the mean of the transfer function values (outputs) is replaced by the transfer function of the mean input

$$\dot{s} = f(\langle \Lambda \rangle) - s, \quad (3)$$

becomes exact. Eq.(3) admits two trivial fixed points corresponding to the quiescent ($s^* = 0$) and saturated ($s^* = 1$) states, respectively. The quiescent (resp. saturated) state is stable

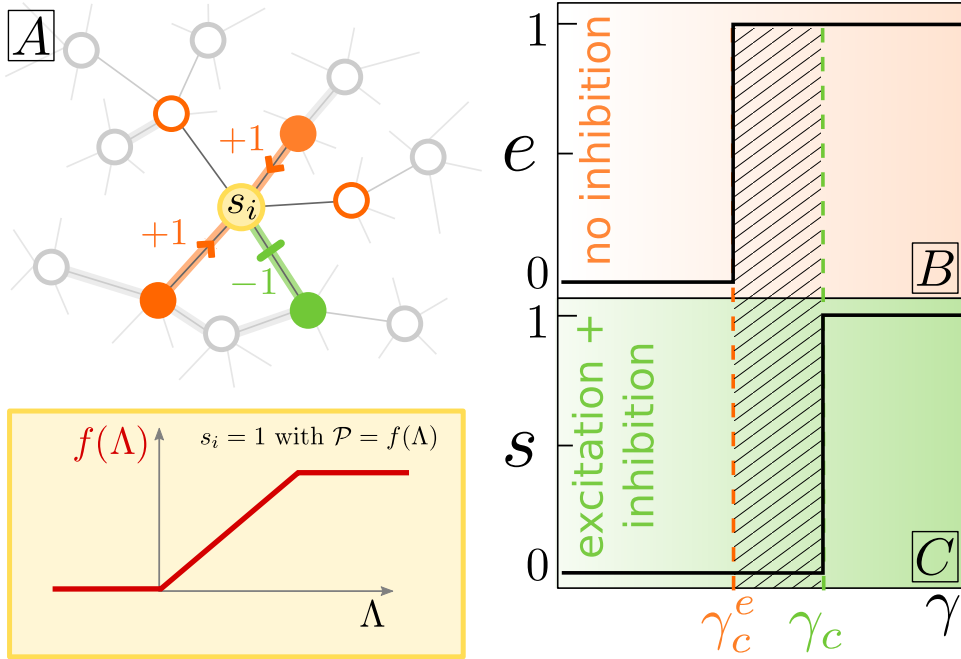


Figure 1: (A) Upper panel: Sketch of the input received by a single node, including excitatory (orange arrows) and inhibitory (green blunt arrows) interactions from active (colored) neighbors. The lower panel shows the considered transfer function for probabilistic activation of nodes as a function of the input. (B) Averaged level of activity in a fully-connected network consisting solely of $N(1 - \alpha)$ excitatory nodes; it exhibits a discontinuous phase transition at $\gamma_c^e(\alpha) = 1/(1 - \alpha)$ separating a quiescent or Down state from an active or Up one. (C) As (B) but for a network consisting of $N(1 - \alpha)$ excitatory and $N\alpha$ inhibitory nodes. Let us remark that the shape of the phase transition depends on our choice for the transfer function. More plausible, non-linear, transfer functions lead e.g. to discontinuous transitions with a region of bistability (phase coexistence) and hysteresis; however, the main results of this work are remain unaffected (see Supplementary Information (SI) 2).

below a given value of the coupling constant, $\gamma < \gamma_c = 1/(1 - 2\alpha)$ (resp. $\gamma > \gamma_c$), while right at γ_c all values of $0 \leq s \leq 1$ are marginally stable. Thus, as illustrated in Fig.1B, the system experiences a discontinuous phase transition at γ_c (i.e. the all-or-none phenomenon described in the Introduction). Observe also (see Fig.1C) that, in agreement with intuition, as the fraction of inhibitory nodes in the network is increased (i.e. as α grows), the overall level of activity tends to decrease, and the nature of the phase transition is not altered: it remains discontinuous even in the presence of inhibitory populations.

1.3 Beyond mean-field: Sparse networks

Computational analyses of the model on sparse networks reveal a phenomenology much richer than the just described mean-field one. As shown in Fig.2 the phase transition becomes progressively smoother (continuous) as the network connectivity k is reduced, and a novel intermediate phase where the overall average activity s does not saturate to either 0 or 1 emerges. Importantly, let us stress that such an intermediate phase does not appear in sparse networks of purely excitatory nodes.

To gauge the level of network-state variability, we measured computationally the standard deviation σ_s of \bar{s} (average of s finite-time windows for finite-size networks; see Fig.2) over realizations. This quantity exhibits two marked peaks (Fig.2) suggesting the existence of two phase transitions [40, 2]. The (leftmost) peak, at γ_c^e , corresponds to a transition from the

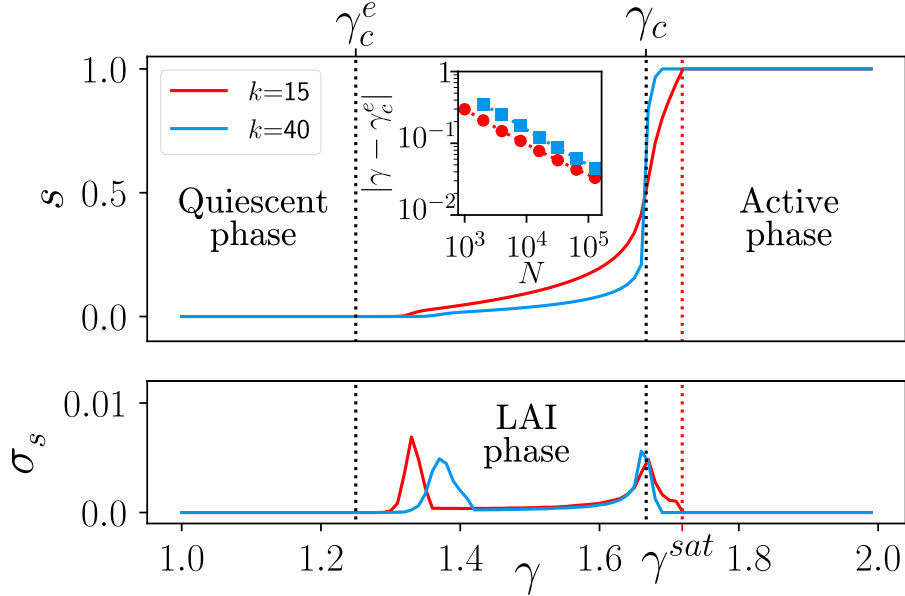


Figure 2: Overall steady-state averaged network activity s for the E/I model on a sparse hyper-regular network ($N = 16000$) in which all nodes have the same (in-)connectivity k (with either $k = 15$ or $k = 40$) and the same fraction of $((1 - \alpha)k)$ excitatory and (αk) inhibitory inputs ($\alpha = 0.2$ here). (A, Bottom) Variance across (10^3) runs of the total network activity averaged in time windows of a given length ($T = 10^4$ MonteCarlo steps) as a function of the coupling strength γ for two different values of the connectivity k ; each curve shows two marked peaks, indicative of two phase transitions. The leftmost one, $\gamma_c^e(k, N)$, shifts towards γ_c^e in the large- N limit, obeying finite-size scaling, as illustrated by the straight line in the double-logarithmic plot of the inset. On the other hand, the second peak is a remanent of the mean-field first-order transition at $\gamma_c = 1/(1 - 2\alpha) = 1.66\dots$ and is hardly sensitive to finite-size effects.

quiescent ($s = 0$) to the *low-activity intermediate (LAI)* phase. Observe that, γ_c^e exhibits severe finite-size-scaling corrections (depending also on k) converging to $\gamma_c^e = 1/(1 - \alpha)$ as $N \rightarrow \infty$ (see the inset in Fig.2). This value of γ coincides with the mean-field transition point for the purely excitatory subnetwork with $N(1 - \alpha)$ units (i.e. without inhibition; see Fig.1A), justifying the superindex e in γ_c^e . On the other hand, the second peak is located at $\gamma_c = 1/(1 - 2\alpha)$, i.e. the very same location of the mean-field discontinuity for the fully-connected network. These two transition points delimit the LAI phase. There is a third relevant value, $\gamma = \gamma^{sat}$ (within the active phase) at which the fully-saturated solution, $s = 1$, emerges. As k increases, this third point becomes closer to γ_c , making the second transition progressively sharper and converging to the mean-field result.

1.4 Analytical results for sparse networks

To rationalize the novel (LAI)phase with low levels of activity, it is essential to realize that, in the sparse-connectivity case, the input received by a given node does not necessarily take its mean-field value, but is a fluctuating variable, making it thus necessary to consider Eq.(2) rather than its mean-field counterpart Eq.(3). To make analytical progress it is necessary to determine the input distribution, which is equivalent to computing the probability $p_{lj}(s)$ that a given node has exactly l active inhibitory neighbors and j active excitatory ones, for arbitrary values of l and j .

Larremore *et. al.* made an attempt to solve this problem working with the actual (“quenched”)

network architecture, which requires scrutinizing the (spectral) properties of the associated connectivity matrices [11]. Here, we propose to tackle the problem from a complementary angle. More specifically, we consider a random-neighbor (“annealed”) network version of the model, in which, at each time step, the neighbors of each node are randomly sampled from the whole network (keeping fixed the number of them as well as the fractions of excitatory and inhibitory ones). This annealed variant of the model greatly simplifies the analytical calculations, and – quite surprisingly – leads to results identical (up to numerical precision) to those for the original quenched-network problem.

For the annealed version of the model one can readily write (see SI-3):

$$p_{lj}(s) = \binom{k\alpha}{l} \binom{k(1-\alpha)}{j} s^{j+l} (1-s)^{k-j-l}, \quad (4)$$

which depends solely on s , i.e. the probability for any arbitrary node to be active. From this, it follows that

$$\langle f(\Lambda) \rangle = \sum_{l,j} p_{lj}(s) f[\tilde{\gamma}(j-l)], \quad (5)$$

(where $\tilde{\gamma} = \gamma/k$), as well as $\langle \Lambda \rangle = \gamma(1-2\alpha)s$ and $\sigma^2(\Lambda) = \gamma^2 s(1-s)/k$ for the mean and the variance of the input distribution, respectively. Note that all these are functions of s and $\tilde{\gamma}$, solely. Evaluating Eq.(5) is not straightforward owing to the non-linearity of f . However, analytical insight can be obtained by Taylor-expanding around either of the two trivial solutions: $s^* = 0$ or $s^* = 1$. Expanding around $s^* = 0$ and keeping only leading order (linear in s) contributions, leads to $\langle f(\Lambda) \rangle \simeq f(\tilde{\gamma}k(1-\alpha)s)$, which plugged into Eq.(2) implies that the solution $s^* = 0$ loses its stability at a critical point $\gamma_c^e = 1/(1-\alpha)$, in perfect agreement with the computational observations (for $N \rightarrow \infty$) Observe that the LAI noise-induced phase exists for all finite connectivity values and emerges at γ_c^e for all k , but –owing to finite-size corrections– larger and large networks are required to see it as the network connectivity is increased.

A similar analysis around $s^* = 1$ (see SI-4) reveals that the saturated solution is stable only above

$$\gamma^{sat} = \frac{1 - k(1-\alpha)}{(1-\alpha) - k(1-\alpha)(1-2\alpha)}, \quad (6)$$

again in perfect agreement with numerical findings (see Fig.2 and SI-4). As expected γ^{sat} converges to the mean-field prediction $1/(1-2\alpha)$ for $k \rightarrow \infty$, as numerically observed.

Thus, contrarily to mean-field expectations, there exists a whole intermediate region, $\gamma_c^e < \gamma < \gamma^{sat}$, where activity does not vanish nor saturate for E/I networks. Such a region emerges as a consequence of input fluctuations and, hence, stems from network sparsity. Observe that for purely excitatory networks, i.e. with $\alpha = 0$, $\gamma_c^e = \gamma^{sat}$ and the intermediate region vanishes.

1.5 Jensen’s force

To go beyond perturbative results, note that the difference between the exact equation for the model on a sparse network, Eqs.(2), and its mean-field approximation, Eqs.(3), is that $\langle f(\Lambda) \rangle \neq f(\langle \Lambda \rangle)$, i.e. the non-linear function f and the network average are non-commuting “operators”, and the reported non-trivial effects for sparse networks necessarily stem from the difference between them:

$$F(\tilde{\gamma}, s) \equiv \langle f(\Lambda) \rangle - f(\langle \Lambda \rangle). \quad (7)$$

Observe that, as the terms in the r.h.s. depend on s , $F(\tilde{\gamma}, s)$ is state-dependent stochastic force. As shown above (and as suggested by the central limit theorem) the distribution of inputs to any given node is centered at $\langle \Lambda \rangle$ and has a standard deviation that scales as $1/\sqrt{k}$. If f was a linear function, then $\langle f(\Lambda) \rangle = f(\langle \Lambda \rangle)$, but as it is a convex function near the origin, then

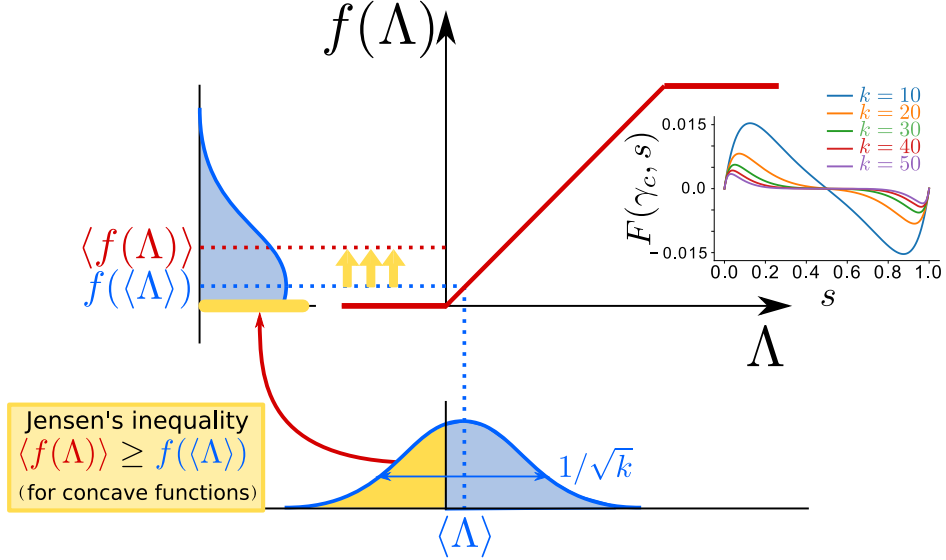


Figure 3: Sketch illustrating the origin of the noise-induced Jensen’s force. Each node in a sparse network receives an input Λ which is a random variable extracted from some bell-shaped probability distribution function $P(\Lambda)$ (sketched below the x-axis) with averaged value $\langle \Lambda \rangle = \gamma(1 - 2\alpha)s$ and standard deviation $\sigma_s = (\gamma\sqrt{s(1-s)})/\sqrt{k}$ (see SI-3). The possible outputs $f(\Lambda)$ are also distributed according to some probability (sketched to the left of the y-axis). Given that around $\Lambda \approx 0$ the function $f(\Lambda)$ is locally convex then, as a consequence of Jensen’s inequality for convex functions, $\langle f(\Lambda) \rangle \geq f(\langle \Lambda \rangle)$ (i.e. the dotted red line is above the blue one). Indeed, while for positive inputs, the transformation is linear, negative ones are mapped into 0 thus creating a net positive Jensen’s force for small values of Λ (or s). The inset shows the Jensen’s force $F(\tilde{\gamma}, s) \equiv \langle f(\Lambda) \rangle - f(\langle \Lambda \rangle)$ computed right at the critical point γ_c for different connectivity values, as a function of s . Note, the negative values for large values of s which stem from the concavity of the function $f(x)$ around $x = 1$. Note that F decreases as k grows and vanishes in the mean-field limit.

the Jensen’s inequality of probability theory (which expresses the fact that if x is a random variable and $g(x)$ is a convex function, then $\langle g(x) \rangle \geq g(\langle x \rangle)$) implies that $\langle f(\Lambda) \rangle > f(\langle \Lambda \rangle)$, i.e. F is positive if $\langle \Lambda \rangle$ is near the 0, i.e. if s is relatively small.

Thus, we propose the term “Jensen’s force” to refer to $F(\tilde{\gamma}, s)$ (see Fig.3). This positive force is responsible for the destabilization of the quiescent state and the emergence of the LAI phase. Observe that if, on the other hand, $\langle \Lambda \rangle$ happens to be close to 1, the function f is locally concave and, using a reverse argument, $\langle f(\Lambda) \rangle < f(\langle \Lambda \rangle)$, i.e. there is a negative Jensen’s force F in the regime of very large activities (justifying the reduction of the saturated regime with respect to the mean-field case). Finally, if parameters are such that the system lies in the quiescent ($s = 0$) or in the saturated ($s = 1$) phase then there are no input fluctuations –i.e. the input distribution is delta function– and the Jensen’s force vanishes.

$F(\tilde{\gamma}, s)$ can be analytically calculated for some particular transfer functions f (see SI-5) but, in general, it can be only determined numerically. For the sake of illustration, results for the function f considered in Eq.(1) are shown in the Fig.3 (inset) for the particular case $\gamma = \gamma_c$. Observe that $F(\tilde{\gamma}, s)$ is positive for $s < 1/2$, negative for $s > 1/2$ and vanishes at $s = 1/2$ explaining why the steady state is precisely $s = 1/2$ at γ_c . Similar arguments work for other values of $\tilde{\gamma}$. Let us emphasize that the magnitude of the force decreases as k grows (Fig.3, inset) vanishing in the limit in which networks are no longer sparse.

Summing up, the sparsity-induced Jensen’s force F is responsible for the emergence of a LAI phase in E/I networks below the mean-field critical point, γ_c as well as for a reduction in

the overall level of activity with respect to the mean-field limit in a region above γ_c .

Let us emphasize that the annealed-network approximation fits perfectly well all computational results obtained for quenched networks, with fixed neighbors and intrinsic structural disorder (we have computationally verified that, indeed, the quenched and the annealed versions of the model give identical results; see SI-5). The reason for this agreement, lies in the absence of node-to-node correlations within the LAI phase (see below), which suggests that the annealed approximation is exact in the large-network limit. For the sake of completeness, we have computationally verified that the LAI phase emerges also for other (non-linear) transfer functions, more random (non hyper-regular) networks as well as for heterogeneous weight distributions (see SI-5).

1.6 Phase transitions from and to the LAI phase

Fig.2 reveals the existence of two phase transitions, one at each side of the LAI phase. Around the left-most one, at γ_c^e , we performed standard analyses of avalanches, by introducing a single seed of activity (one active excitatory node) in an otherwise quiescent state, and analyzed the statistics of the cascades of activations it triggers. For both, avalanche sizes and avalanche durations, we measured scale-free distributions with the standard exponents of the unbiased branching process [41, 42] (see SI-6). This is not surprising given the un-structured nature of the network. Further analyses need to be done in lower dimensional systems to see if this transition from a quiescent to a noise-induced active phase shares the critical features of standard quiescent-to-active phase transitions (known to be in the so-called directed percolation universality class [2, 3]) or if novel behavior emerges owing to noise-induced effects. On the other hand, the second phase transition, at $\gamma_c = 1/(1 - 2\alpha)$ is a remnant of the original (discontinuous) mean-field one, and signals a (continuous) transition between states of low activity to high activity ones. This phase transition also needs further scrutiny to be fully elucidated. A detailed analysis of these phase transitions, as well as of their possible relevance in connection with the hypothesis that the cerebral cortex might operate at the edge of a critical point [41, 43, 44, 4, 37] is left as an open challenge for future work (see Discussion).

1.7 Asynchronous-state features

The cortical *asynchronous* state is characterized by a number of key features (see also Methods) including: **i)** Large variability: the coefficient of variation, CV , defined as the ratio of the standard deviation to the mean of the interspike intervals (i.e. periods of un-interrupted silence for a given neuron/node) is large, i.e. $CV \geq 1$ [14]. **ii)** The network-averaged pairwise Pearson's correlation coefficient PC is very low; actually it decays to 0 with network size reflecting a lack of synchronization or coherent behavior [32, 45, 25]. **iii)** There is a (short) time lag between excitation and inhibition (E-I lag) meaning that an excess in excitation is rapidly compensated by an increase in inhibitory activity, so that inhibition actively de-correlates neural populations and the network state remains stable, as theoretically predicted [25, 46, 47, 48] and experimentally confirmed [49, 17].

As shown in Fig.4 the LAI phase –but not the quiescent nor the active ones– displays all these key features (see figure caption for details). Moreover, in agreement with the original claim for asynchronous states [21, 22], we verified that all along the LAI phase (and only in the LAI phase) the dynamics is chaotic (or quasi-chaotic) in the sense of damage spreading dynamics [50] (see SI-7). Thus, in synthesis, all the chief features of cortical asynchronous states are also distinctive and exclusive characteristics of the LAI phase.

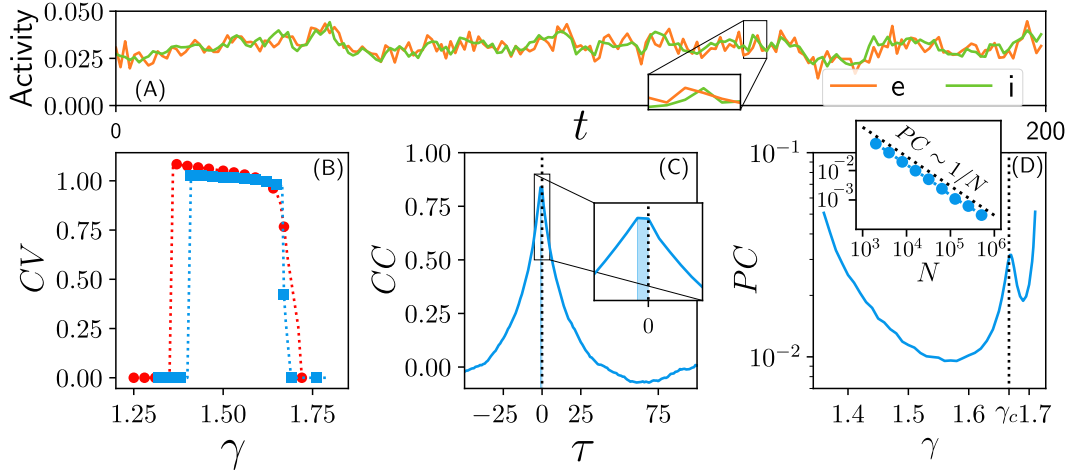


Figure 4: (A) Time series of the excitatory (e; orange line) and inhibitory (i; green line) network activity in the LAI phase (network $N = 16,000$). The zoom illustrates the small (one-time step) E-I lag present in this phase. (B) Coefficient of variation (CV) vs. coupling-strength γ ; $CV \geq 1$ within the LAI phase, while it vanishes in the quiescent and active phases (the color code, as in Fig.2, stands for connectivity values). (C) Time-lagged cross-correlation (CC) between the excitation and inhibition timeseries in the LAI phase. The maximum (black dashed line) reflects the existence of a one-step E-I lag. (D) Pairwise Pearson's correlation (PC) between nodes in the LAI phase as function of γ ; it takes small values, but exhibits a marked peak at the critical point γ_c (dotted line). The inset shows that the PCs scale with system size as $1/N$ thus vanishing in the large-network limit (data for $\gamma = 1.55$, but results valid all across the LAI phase).

1.8 Tightly-balanced networks

We now scrutinize how the region in parameter space in which the LAI phase emerges can be maximized, thus limiting the need for parameter fine tuning to exploit the possible functional advantages of such a regime. This is achieved by considering *tightly-balanced* networks (also called detailed-balanced networks) [51, 20] in which excitatory and inhibitory inputs are tuned to compensate mutually, so that the average input of individual nodes is kept close to 0. To do so, it suffices to introduce in the model definition, Eq.(1), two different strengths for excitatory and inhibitory synapses, ω^e and ω^i . In this way, the (leftmost) transition point is shifted to, $\gamma_c^e = 1/(\omega^e(1 - \alpha))$, while γ_c changes to

$$\gamma_c = \frac{1}{(\omega^e(1 - \alpha) - \omega^i\alpha)} \quad (8)$$

which diverges to infinity if $\omega^e/\omega^i = \alpha/(1 - \alpha)$, implying that the largest possible LAI phase is obtained when such a condition is met (observe that in such a limit the level of activity varies very slowly converging to $s = 1/2$ as $\gamma \rightarrow \infty$). But, given that $e/(1 - \alpha) = i/\alpha$, the above condition corresponds precisely to the tightly-balanced networks for which the averaged input of each single node, $\langle \Lambda \rangle = \tilde{\gamma}(\omega^e e - \omega^i i)$, vanishes. Thus, tightly-balanced networks have the largest possible LAI phase and the largest possible dynamic range.

1.9 Experimental measurements of the LAI phase and the Jensen's force

Is it possible to measure the Jensen's force experimentally? We believe it is, but explicitly designed setups would be required. First of all, let us recall that asynchronous states (i.e. LAI phases) have been detected experimentally both *in vivo* and *in vitro* [28, 30, 27]. Importantly,

with today’s technology, the spiking activity of more than 1000 neurons can be measured simultaneously (see e.g. [52]), so that much better statistics can be collected. In principle, one should be able to compute the Jensen’s force in this type of experiments. In SI-8 we propose a tentative experimental protocol to do so. However, we leave this programme for future research as well as an open challenge for experimentalists.

Conclusions and Discussion

It has been long observed that neurons in the brain cortex remain active even in the absence of stimuli [14, 15, 16]. Often, such a sempiternal spontaneous activity is steady and highly-irregular –the so-called asynchronous state– while in some other circumstances, depending mostly on cortical region and functional state, diverse levels of synchronization across the asynchronous-synchronous spectrum are observed [33, 23].

While the role of synchronization in neuronal networks has been long studied [53], the role of the asynchronous state remained more elusive [25]. Presently, it has become widely shown that the asynchronous state emerges from the interplay between excitation and inhibition, and that it is essential for network stability and to allow for high computational capabilities [17, 18, 19].

Our main goal here was to investigate the origin low-activity regimes in excitation/inhibition networks, determining in particular the nature of their (thermodynamic) phases. For this, we employed a statistical-mechanics viewpoint and searched for a modelling approach as parsimonious as possible, i.e. a sort of Ising model of E/I networks. In particular, we analyzed a model which further simplifies the one proposed by Larremore *et al.* [11] in a few different ways. For example, we removed network heterogeneity both in its architecture and in the allowed synaptic weights to allow for mathematical tractability.

Our main result is that E/I networks exhibit a non-trivial LAI phase in between standard quiescent and active phases, in which activity reverberates indefinitely without the need of external driving, nor of intrinsically firing neurons (in contradictions to many previous beliefs). Such LAI phase stems purely from fluctuations and, thus, have little to do with the specific network structure. In particular, this disproved an initial conjecture of us suggesting that intermediate levels of activity could be related to so-called *Griffiths phases*. Such phases have remarkable features [54] and have been claimed to be relevant for cortical dynamics [55]; they also emerge in between quiescent and active phases, but only in systems characterized by structural heterogeneity and, thus, are unrelated to the novel LAI phase uncovered here. Nevertheless, an important research line left for future work, is to analyze how the properties of the LAI phase are altered in more structured and realistic networks including e.g. broad degree distributions, clustered structure and modular-hierarchical organization, which might lead to novel phenomena [56, 57, 58, 55].

Two key ingredients are necessary for the LAI phase to emerge: a spontaneously generated dynamical balance between excitation and inhibition and network sparsity. The resulting phase has all the statistical properties usually ascribed to asynchronous states.

An issue worth discussing is the dependence of the presented phenomena on network connectivity and the connection of our work with the standard view of balanced networks as originally proposed in the seminal work of van Vreeswijk and Sompolinski[21]. As we showed, the LAI phase emerges out of input fluctuations and –as the input standard deviation scales with γ/\sqrt{k} – it relies crucially on the finiteness of k , i.e. on network sparsity. However, it is important to underline that, as we showed, the LAI phase survives even for arbitrarily large values of k , but larger and larger network sizes N are required for it to be evident. However, it is also possible to adopt the original scaling proposed in [21], where it was argued that if the strength of individual synapses is of order $1/\sqrt{k}$ (rather than constant as here), it compensates fluctuations in the number of actual inputs (order \sqrt{k}), leading a total input fluctuations of the same order of the neuron firing threshold (order unity), and thus to fluctuation-controlled activations. This type

of scaling can be easily accommodated within our approach just by replacing γ/k in Eq.1 by γ'/\sqrt{k} ; with this scaling, the critical points in terms of the new coupling constant γ' are shifted as k grows, and the noise-induced phase persists even in the limit of non-sparse networks. Note also that, as illustrated here, having a sharp threshold is not a necessary ingredient for the phenomenon to occur: the LAI phase also emerges when considering, e.g. a transfer function such as the hyperbolic-tangent without a hard discontinuity. In other words: the Jensen’s force is more general than a hard threshold, noise-filtering, mechanism.

In order to verify whether more realistic neuronal networks models exhibit also an intermediate phase, in between quiescent and standard active ones, we first scrutinized the recent literature. We found that there are two recent computational analyses of E/I networks of integrate-and-fire neurons with (current-based or conductance-based) synapses confirming the emergence of a similar self-sustained intermediate regime with high variability [34, 35]. This confirms that the very general mechanism put forward here also applies to more detailed/complicated neuron models. Furthermore, the concept of Jensen’s force sheds light on the computational findings of these recent works.

We have also proposed a tentative protocol to challenge experimentalist to empirically measure Jensen’s forces in actual neuronal networks, either *in vivo* or *in vitro*. Even if technical difficulties are likely to emerge, we strongly believe that Jensen’s forces are susceptible to be observed and quantified in the lab. This research programme, if completed, would strongly contribute to shedding light on the noisy dynamics of cortical networks, as well as on the way it helps processing information.

Let us also comment on the relationship between the so called “criticality hypothesis” –i.e. the idea that the cortex, as well as some other biological systems, might extract important functional advantages from operating near the critical point of a continuous phase transition [41, 43, 36, 59, 4, 37]– and the findings in this work. Let us emphasize that asynchronous states and critical states have almost opposite features: the first is characterized by active de-correlation of nodes and the second exhibits strong system-spanning correlations. Thus Clarifying the interplay between these two antagonistic interpretations/phenomena –and analyzing them together within a unified framework– is a challenging goal [60, 61]. We believe that our simple model (probably improved with further important ingredients such as some form of synaptic plasticity (as e.g. in [37])) is a good candidate to constitute a unified framework to put together asynchronous and synchronous states and the critical phase transition in between, and to analyze these fundamental questions. Observe in particular that the LAI phase is separated from the quiescent and active phases, respectively, by continuous phase transitions –including critical points– whose specific details still need to be further elucidated. As a matter of fact, having a good understanding of the main phase transitions of E/I networks is a fundamental preliminary step to make solid progress to contribute to the criticality hypothesis.

Finally, let us mention that we are presently exploring the possibility of observing similar LAI phases in other biological networks such as gene regulatory ones, where gene repression plays a role equivalent to synaptic inhibition in neural networks where opposite conflicting influences may mutually compensate to each other, leading to noise-induced phenomena. We hope that the novel stochastic force and phase elucidated here foster new research along and this and similar lines.

Methods

Some of the most relevant methods have been sketched in the main text. Here we detail some important methodological aspects. Further details are provided in the Supplementary information (SI).

Hyper-regular networks

For the sake of mathematical tractability, we consider hyper-regular networks in which each node has exactly $k_{exc} = k(1 - \alpha)$ excitatory neighbors and $k_{inh} = k\alpha$ inhibitory ones pointing to it (where α is the fraction of inhibitory nodes). For this, we follow these steps: (i) two random regular networks, one of excitatory nodes with connectivity k_{exc} and one of inhibitory units with connectivity k_{inh} are generated; (ii) $k^e = k(1 - \alpha)$ links (avoiding node repetitions) are randomly chosen to point to each inhibitory node. This process got sometimes stuck due to a topological conflict, so we re-started the process after 10^6 unsuccessful attempts to include new links. Each link of the so constructed networks is taken with positive weight for interactions from an excitatory node j to an inhibitory neuron i ($\omega_{ij} > 0$) and negative for the opposite interaction ($\omega_{ji} < 0$). On the other hand, all weights within the excitatory (resp. inhibitory) subnetwork are positive (resp. negative). For the purpose of illustration a hyper-regular network is shown in SI-1.

Mean field approach

The excitatory and inhibitory populations (E,I) evolve stochastically according to a Master equation [62] described by the following transition rates for large networks:

$$\begin{aligned}
 \Omega(E, I \rightarrow E + 1, I) &= [N(1 - \alpha) - E] \langle f(\Lambda) \rangle \\
 \Omega(E, I \rightarrow E - 1, I) &= E [1 - \langle f(\Lambda) \rangle] \\
 \Omega(E, I \rightarrow E, I + 1) &= [N\alpha - I] \langle f(\Lambda) \rangle \\
 \Omega(E, I \rightarrow E, I - 1) &= I [1 - \langle f(\Lambda) \rangle]
 \end{aligned} \tag{9}$$

where the timescale has been set to unity, $\langle f(\Lambda) \rangle$ is the average probability for any given node to become active ($\langle \cdot \rangle$ stands for network average), and factors such as $N(1 - \alpha) - E$ (resp. $(N\alpha - I)$) describe the number of inactive excitatory (resp. inhibitory) nodes. Performing a $1/N$ expansion of the corresponding Master equation [62] and keeping terms up to leading-order, one readily obtains the following deterministic equations:

$$\begin{cases} \dot{e} = (1 - \alpha) \langle f(\Lambda) \rangle - e \\ \dot{i} = \alpha \langle f(\Lambda) \rangle - i \end{cases}$$

where the dot stands for time derivative for $e = E/N$ and $i = I/N$, respectively. In particular, considering a fully-connected system in the large size limit (i.e. $N \rightarrow \infty$), fluctuations in the input of each node are negligible. Thus, all nodes receive the same input, and the mean of the transfer function values is replaced by the transfer function of the mean input, i.e. the mean-field approach implies

$$\langle f(\Lambda) \rangle = f(\langle \Lambda \rangle) \tag{10}$$

The detailed procedure to compute these averages is presented in SI-4.

Asynchronous-state features

Coefficient of variation It is defined as the quotient of the standard deviation σ_{ISI} to the mean μ_{ISI} of the inter-spike interval (*ISI*) on individual units:

$$CV = \frac{\sigma_{ISI}}{\mu_{ISI}}. \tag{11}$$

Excitatory/inhibitory cross-correlation Given two time series $x(t)$ and $y(t)$, the Pearson correlation coefficient of $x(t)$ and $y(t + \tau)$

$$CC(\tau) = \frac{1}{\sigma_x \sigma_y} \sum_{\tau=-\infty}^{+\infty} \overline{x(t)y(t + \tau)}. \quad (12)$$

where σ_x and σ_y are the standard deviations of the time series $x(t)$ and $y(t)$, respectively and τ is a time delay. Since we are interested in the E/I lag, we subtract the mean from the time series, i.e. we take $x(t) = e(t) - \mu_e$ and $y(t) = i(t) - \mu_i$. This procedure ensure us a correct normalization, so $CC(\tau) \in [-1, 1]$. In this way, if $CC(\tau)$ has a peak for $\tau < 0$, we conclude that the activity of the inhibitory population resembles the activity of the excitatory one, but it is shifted to the left: excitatory population spikes first and it is followed by the inhibitory one.

Pairwise correlation The Pearson's correlation coefficient between a randomly selected pair of nodes in the network, x_i and x_j , is defined as

$$PC_{x_i, x_j} = \frac{\langle x_i x_j \rangle - \langle x_i \rangle \langle x_j \rangle}{\sqrt{\langle x_i^2 \rangle - \langle x_i \rangle^2} \sqrt{\langle x_j^2 \rangle - \langle x_j \rangle^2}} \quad (13)$$

where $\langle \cdot \rangle$ represents a temporal average. The total Pearson's correlation coefficient (PC) is computed by averaging PC_{x_i, x_j} over 500 pairs of nodes for different realizations.

Chaotic behavior It is important to scrutinize the possible chaotic nature of the LAI phase [21]. For this, we employ the standard method (particular results are shown in SI-7), consisting in analyzing the dynamics of damage spreading [50]. The method involves the next steps: (1) take a specific state of a network, M , and a construct an identical replica of it, M' , in which the state of only a randomly-chosen node is changed; (2) the Hamming distance, H –defined as the difference of states between M and M' – is commuted after one time step (i.e. an update of all the nodes of the two networks) and finally, (3) H is averaged over many realizations (i.e. over different locations of the initial damage and stochastic trajectories) obtaining the branching parameter, B . If $B < 1$ perturbations tend to shrink and the network is in a ordered phase, while if $B > 1$ perturbations growth on average and the network exhibit chaotic-like behavior. Finally, for marginal propagation of perturbations, i.e. $B = 1$, the network is critical.

Acknowledgments

We acknowledge the Spanish Ministry of Science as well as the Agencia Española de Investigación (AEI) for financial support under grant FIS2017-84256-P (FEDER funds). V.B and R.B. acknowledge funding from the INFN BIOPHYS project. We warmly thank P. Moretti, J. Mejias, for very useful comments. This work is dedicated to the memory of Prof. Daniel Amit, who shared with us (MAM), his passion for understanding cortical fluctuations before this was a popular research topic.

References

- [1] Pastor-Satorras, R., Castellano, C., Van Mieghem, P. & Vespignani, A. Epidemic processes in complex networks. *Rev. Mod. Phys.* **87**, 925 (2015).
- [2] Henkel, M., Hinrichsen, H. & Lubeck, S. *Non equilibrium Phase Transitions: Absorbing phase transitions*. Theor. and Math. Phys. (Springer, Berlin, 2008).

- [3] Marro, J. & Dickman, R. *Nonequilibrium Phase Transition in Lattice Models* (Cambridge Univ. Press, 1999).
- [4] Muñoz, M. A. Colloquium: Criticality and dynamical scaling in living systems. *Rev. Mod. Phys.* **90**, 031001 (2018).
- [5] Wilson, H. R. & Cowan, J. D. Excitatory and inhibitory interactions in localized populations of model neurons. *Biophys. J.* **12**, 1–24 (1972).
- [6] Davidson, E. & Levin, M. Gene regulatory networks. *Proc. Natl. Acad. of Sci. (USA)* **102**, 4935–4935 (2005).
- [7] Ozbudak, E. M., Thattai, M., Lim, H. N., Shraiman, B. I. & Van Oudenaarden, A. Multistability in the lactose utilization network of escherichia coli. *Nature* **427**, 737 (2004).
- [8] Isaacson, J. S. & Scanziani, M. How inhibition shapes cortical activity. *Neuron* **72**, 231–243 (2011).
- [9] Tyson, J. J., Chen, K. C. & Novak, B. Sniffers, buzzers, toggles and blinkers: dynamics of regulatory and signaling pathways in the cell. *Curr. Opin. Cell Biol.* **15**, 221–231 (2003).
- [10] Chen, X. & Dzakpasu, R. Observed network dynamics from altering the balance between excitatory and inhibitory neurons in cultured networks. *Phys. Rev. E* **82**, 031907 (2010).
- [11] Larremore, D. B., Shew, W. L., Ott, E., Sorrentino, F. & Restrepo, J. G. Inhibition causes ceaseless dynamics in networks of excitable nodes. *Phys. Rev. Lett.* **112**, 138103 (2014).
- [12] Liu, B.-h. *et al.* Broad inhibition sharpens orientation selectivity by expanding input dynamic range in mouse simple cells. *Neuron* **71**, 542–554 (2011).
- [13] Pouille, F., Marin-Burgin, A., Adesnik, H., Atallah, B. V. & Scanziani, M. Input normalization by global feedforward inhibition expands cortical dynamic range. *Nat. Neurosci.* **12**, 1577 (2009).
- [14] Softky, W. R. & Koch, C. The highly irregular firing of cortical cells is inconsistent with temporal integration of random epsps. *J. Neurosci.* **13**, 334–350 (1993).
- [15] Arieli, A., Sterkin, A., Grinvald, A. & Aertsen, A. Dynamics of ongoing activity: explanation of the large variability in evoked cortical responses. *Science* **273**, 1868–1871 (1996).
- [16] Abeles, M. *Corticonics: Neural circuits of the cerebral cortex* (Cambridge University Press, 1991).
- [17] Sippy, T. & Yuste, R. Decorrelating action of inhibition in neocortical networks. *J. Neurosci.* **33**, 9813–9830 (2013).
- [18] Vogels, T. P., Sprekeler, H., Zenke, F., Clopath, C. & Gerstner, W. Inhibitory plasticity balances excitation and inhibition in sensory pathways and memory networks. *Science* **334**, 1569–1573 (2011).
- [19] Rubin, R., Abbott, L. F. & Sompolinsky, H. Balanced excitation and inhibition are required for high-capacity, noise-robust neuronal selectivity. *Proc. Natl. Acad. of Sci. (USA)* 201705841 (2017).
- [20] Denève, S. & Machens, C. K. Efficient codes and balanced networks. *Nat. Neurosci.* **19**, 375 (2016).

- [21] Van Vreeswijk, C. & Sompolinsky, H. Chaos in neuronal networks with balanced excitatory and inhibitory activity. *Science* **274**, 1724–1726 (1996).
- [22] Vreeswijk, C. v. & Sompolinsky, H. Chaotic balanced state in a model of cortical circuits. *Neural Comput.* **10**, 1321–1371 (1998).
- [23] Brunel, N. Dynamics of sparsely connected networks of excitatory and inhibitory spiking neurons. *J. Comput. Neurosci.* **8**, 183–208 (2000).
- [24] Brunel, N. & Hakim, V. Sparsely synchronized neuronal oscillations. *Chaos* **18**, 015113 (2008).
- [25] Renart, A. *et al.* The asynchronous state in cortical circuits. *Science* **327**, 587–590 (2010).
- [26] Shu, Y., Hasenstaub, A. & McCormick, D. A. Turning on and off recurrent balanced cortical activity. *Nature* **423**, 288 (2003).
- [27] Haider, B., Duque, A., Hasenstaub, A. R. & McCormick, D. A. Neocortical network activity in vivo is generated through a dynamic balance of excitation and inhibition. *J. Neurosci.* **26**, 4535–4545 (2006).
- [28] Treviño, M. Inhibition controls asynchronous states of neuronal networks. *Front. Synaptic Neurosci.* **8**, 11 (2016).
- [29] Dehghani, N. *et al.* Dynamic balance of excitation and inhibition in human and monkey neocortex. *Sci. Rep.* **6**, 23176 (2016).
- [30] Barral, J. & Reyes, A. D. Synaptic scaling rule preserves excitatory–inhibitory balance and salient neuronal network dynamics. *Nat. Neurosci.* **19**, 1690 (2016).
- [31] Lerchner, A. & Latham, P. E. A unifying framework for understanding state-dependent network dynamics in cortex. *arXiv preprint arXiv:1511.00411* (2015).
- [32] Destexhe, A. Self-sustained asynchronous irregular states and up–down states in thalamic, cortical and thalamocortical networks of nonlinear integrate-and-fire neurons. *J. Comput. Neurosci.* **27**, 493 (2009).
- [33] Latham, P. E., Richmond, B. J., Nelson, P. & Nirenberg, S. Intrinsic dynamics in neuronal networks. i. theory. *J. Neurophysiol.* **83**, 808–827 (2000).
- [34] Kriener, B. *et al.* Dynamics of self-sustained asynchronous-irregular activity in random networks of spiking neurons with strong synapses. *Front. Comput. Neurosci.* **8**, 136 (2014).
- [35] Borges, F. *et al.* Self-sustained activity in balanced networks with low firing-rate. *arXiv preprint arXiv:1809.01020* (2018).
- [36] Mora, T. & Bialek, W. Are biological systems poised at criticality? *J. Stat. Phys.* **144**, 268–302 (2011).
- [37] di Santo, S., Villegas, P., Burioni, R. & Muñoz, M. A. Landau–ginzburg theory of cortex dynamics: Scale-free avalanches emerge at the edge of synchronization. *Proc. Natl. Acad. of Sci. (USA)* **115**, E1356–E1365 (2018).
- [38] Newman, M. E. J. The structure and function of complex networks. *SIAM Review* **45**, 167 (2003).
- [39] Soriano, J., Martínez, M. R., Thlusty, T. & Moses, E. Development of input connections in neural cultures. *Proc. Natl. Acad. of Sci. (USA)* (2008).

- [40] Binney, J. J., Dowrick, N. J., Fisher, A. & Newman, M. E. *The Theory of Critical Phenomena* (Oxford University Press, Oxford, 1993).
- [41] Beggs, J. M. & Plenz, D. Neuronal avalanches in neocortical circuits. *J. Neurosci.* **23**, 11167–11177 (2003).
- [42] di Santo, S., Villegas, P., Burioni, R. & Muñoz, M. A. Simple unified view of branching process statistics: Random walks in balanced logarithmic potentials. *Phys. Rev. E* **95**, 032115 (2017).
- [43] Plenz, D. & Niebur, E. *Criticality in neural systems* (John Wiley & Sons, 2014).
- [44] Haimovici, A., Tagliacucchi, E., Balenzuela, P. & Chialvo, D. R. Brain organization into resting state networks emerges at criticality on a model of the human connectome. *Phys. Rev. Lett* **110**, 178101 (2013).
- [45] Harris, K. D. & Thiele, A. Cortical state and attention. *Nat. Rev. Neurosci.* **12**, 509 (2011).
- [46] Ginzburg, I. & Sompolinsky, H. Theory of correlations in stochastic neural networks. *Phys. Rev. E* **50**, 3171–3191 (1994).
- [47] Brunel, N. & Wang, X.-J. What determines the frequency of fast network oscillations with irregular neural discharges? i. synaptic dynamics and excitation-inhibition balance. *J. Neurophysiol.* **90**, 415–430 (2003).
- [48] El Boustani, S. & Destexhe, A. A master equation formalism for macroscopic modeling of asynchronous irregular activity states. *Neural Comput.* **21**, 46–100 (2009).
- [49] Okun, M. & Lampl, I. Instantaneous correlation of excitation and inhibition during ongoing and sensory-evoked activities. *Nat. Neurosci.* **11**, 535 EP (2008).
- [50] Derrida, B. & Pomeau, Y. Random networks of automata: a simple annealed approximation. *EPL* **1**, 45 (1986).
- [51] Vogels, T. P. & Abbott, L. F. Gating multiple signals through detailed balance of excitation and inhibition in spiking networks. *Nat. Neurosci.* **12**, 483 (2009).
- [52] Meshulam, L., Gauthier, J. L., Brody, C. D., Tank, D. W. & Bialek, W. Coarse-graining and hints of scaling in a population of 1000+ neurons. *arXiv preprint arXiv:1812.11904* (2018).
- [53] Buzsáki, G. & Draguhn, A. Neuronal oscillations in cortical networks. *Science* **304**, 1926–1929 (2004).
- [54] Muñoz, M. A., Juhász, R., Castellano, C. & Ódor, G. Griffiths phases on complex networks. *Phys. Rev. Lett.* **105**, 128701 (2010).
- [55] Moretti, P. & Muñoz, M. A. Griffiths phases and the stretching of criticality in brain networks. *Nat. Comm.* **4** (2013).
- [56] Litwin-Kumar, A. & Doiron, B. Slow dynamics and high variability in balanced cortical networks with clustered connections. *Nat. Neurosci.* **15**, 1498 (2012).
- [57] Rosenbaum, R., Smith, M. A., Kohn, A., Rubin, J. E. & Doiron, B. The spatial structure of correlated neuronal variability. *Nat. Neurosci.* **20**, 107 (2017).
- [58] Landau, I. D., Egger, R., Dercksen, V. J., Oberlaender, M. & Sompolinsky, H. The impact of structural heterogeneity on excitation-inhibition balance in cortical networks. *Neuron* **92**, 1106–1121 (2016).

- [59] Shew, W. L., Yang, H., Yu, S., Roy, R. & Plenz, D. Information capacity and transmission are maximized in balanced cortical networks with neuronal avalanches. *J. Neurosci.* **31**, 55–63 (2011).
- [60] Wilting, J. & Priesemann, V. On the ground state of spiking network activity in mammalian cortex. *arXiv preprint arXiv:1804.07864* (2018).
- [61] Stepp, N., Plenz, D. & Srinivasa, N. Synaptic plasticity enables adaptive self-tuning critical networks. *PLoS Comput. Biol.* **11** (2015).
- [62] Gardiner, C. W. *Handbook of stochastic methods: for physics, chemistry and the natural sciences; 3rd ed.* Springer Series in Synergetics (Springer, Berlin, 2004).

Supplementary information: Jensen's force and the statistical mechanics of cortical asynchronous states

Victor Buendía^{1,2,3}, Pablo Villegas¹, Serena di Santo⁴, Alessandro Vezzani^{2,5}, Raffaella Burioni^{2,3}, and Miguel A. Muñoz^{1,2}

¹Departamento de Electromagnetismo y Física de la Materia e Instituto Carlos I de Física Teórica y Computacional. Universidad de Granada. E-18071, Granada, Spain

²Dipartimento di Matematica, Fisica e Informatica, Università di Parma, via G.P. Usberti, 7/A - 43124, Parma, Italy

³INFN, Gruppo Collegato di Parma, via G.P. Usberti, 7/A - 43124, Parma, Italy

⁴Scuola Internazionale Superiore di Studi Avanzati, via Bonomea, 265 - 34136 Trieste, Italy.

⁵IMEM-CNR, Parco Area delle Scienze 37/A - 43124 Parma, Italy

Contents

1	Hyper-regular networks	2
2	Mean-field phase diagram for non-linear transfer functions	2
3	Distribution of the input of an individual neuron for annealed networks	3
4	Derivation of the critical and saturation points	4
5	Robustness of the results	6
6	Avalanches at criticality	10
7	Damage spreading in the asynchronous state	10
8	Experimental measurement of Jensen's force	11

1 Hyper-regular networks

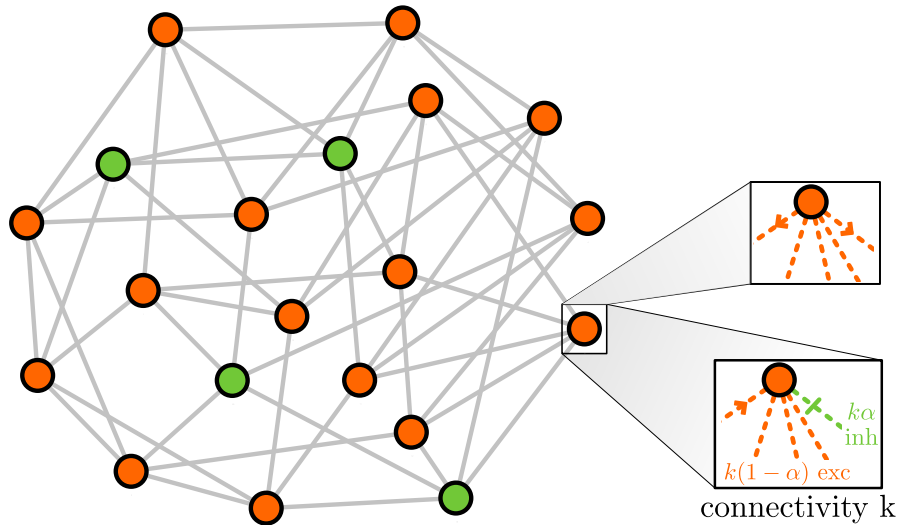


Figure S1: Hyper-regular network with $N = 20$ nodes and connectivity $k = 5$. As in the main text, orange nodes stand for excitation and green nodes for inhibition. For the zoomed node, the difference between out-activity and in-activity is also shown (i.e. each node has $k = 5$ excitatory (or inhibitory) outbound links as well as $k(1 - \alpha)$ excitatory and $k\alpha$ inhibitory inbound links). In particular, each node has, thus, 5 inbound inputs of which 4 are excitatory and 1 inhibitory, as well as 5 outbound links: all of them positive for excitatory units and negative for inhibitory ones.

2 Mean-field phase diagram for non-linear transfer functions

In the mean-field approximation, $\langle f(\Lambda) \rangle \simeq f(\langle \Lambda \rangle) = f(\gamma(1 - 2\alpha)s)$ (see derivation below). Then, the equation for the activity is simply

$$\dot{s} = f(\gamma(1 - 2\alpha)s) - s, \quad (1)$$

which has fixed points $f(\gamma(1 - 2\alpha)s^*) = s^*$. While the position of the critical point γ_c is robust under changes of the transfer function, the stability of the fixed points may change. As a consequence, the shape of the mean-field phase diagram strongly depends on the choice of the transfer function. Since, in mean-field, the activity is bounded to lie in the interval $0 \leq \Lambda \leq 1$, it is possible to Taylor expand $f(\Lambda)$ around $\Lambda = 0$ (which is always a fixed point):

$$f(\Lambda) = a\Lambda + b\Lambda^2 + c\Lambda^3 + \dots \quad (2)$$

where a, b and c are un-specified parameters. This is often called a *Landau expansion* in the theory of critical phenomena [1]. Note that the linear term in Eq.(1) can be absorbed into the a term of Eq.(2), just shifting its value. The signs of the coefficients a, b, c, \dots determine the behaviour of stable fixed points of the system. Fig.S2 shows the phase transition arising from different combinations of these coefficients. In particular, the rightmost figure shows the most realistic case in which there is a region of bistability with hysteresis.

Some of the key properties of these phase transitions persist even for sparse networks, where the LAI phase appears, as shown in Appendix 5.

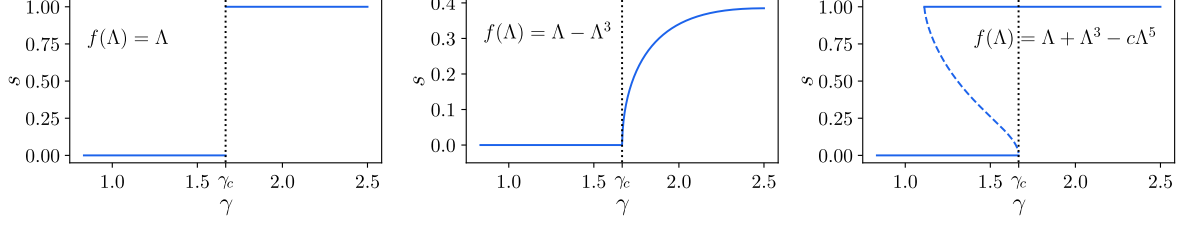


Figure S2: Mean-field phase diagram of Eq.(1) for different choices of the transfer function $f(\langle \Lambda \rangle) = f(\gamma(1 - 2\alpha)s)$. Depending on the signs of the coefficients chosen in the Landau expansion, we may observe discontinuous, continuous, or discontinuous with bistability types of bifurcations (the discontinuous blue line represents unstable fixed points).

3 Distribution of the input of an individual neuron for annealed networks

Here we discuss in detail the derivation of the distribution of inputs received by each individual node within the annealed version of the model. If node has j excitatory active neighbors and l inhibitory active ones, its input is given by $\Lambda_{jl} = \tilde{\gamma}(j - l)$, with $\tilde{\gamma} = \gamma/k$. At each timestep any given node chooses randomly k connecting nodes: n inhibitory and $k - n$ excitatory ones. Thus, the probability to have an input of value Λ_{jl} is controlled by the probability distribution of having j excitatory and l inhibitory active neighbors $p(\Lambda_{jl}|n) = p(j|k - n)p(l|n)$. If the average activity of the network is s , a node picked randomly will be active with probability s , regardless of whether it is excitatory or inhibitory. As a consequence, the probability of finding l active inhibitory neighbors out of the total n inhibitory connections is given by the binomial distribution:

$$p(l|n) = \binom{n}{l} s^l (1 - s)^{n-l}. \quad (3)$$

Similarly, the probability $p(j|n)$ to have a j excitatory active nodes out of $k - n$ possible ones is another binomial distribution. In the case of the hyper-regular model, in which we the number of inhibitory neighbors can be written as $n = k\alpha$ one readily obtains

$$\begin{aligned} p(\Lambda_{jl}) &= \sum_n \delta_{n,k\alpha} p(\Lambda_{jl}|n) = \\ &= \binom{k\alpha}{l} \binom{k(1 - \alpha)}{j} s^{j+l} (1 - s)^{k-j-l}, \end{aligned} \quad (4)$$

(while for regular but not hyper-regular networks this expression becomes more involved). Note that the above probability depends exclusively on the average activity of the network, s , and the connectivity k , so $p(\Lambda_{jl}) \equiv p_{lj}(s)$, as defined in the main text. From this, it is possible to evaluate the averages of any function of the input. In particular, the first and second moments of the input can be easily computed

$$\begin{aligned} \langle \Lambda \rangle &= \sum_{j=0}^{k-n} \sum_{l=0}^n p_{lj}(s) \Lambda_{jl} = \tilde{\gamma} k s (1 - 2\alpha) = \gamma s (1 - 2\alpha) \\ \langle \Lambda^2 \rangle &= \tilde{\gamma}^2 [k s^2 ((1 - 2\alpha)^2 k - 1) + k s], \end{aligned}$$

and, similarly, for the variance

$$\sigma^2(\Lambda) = \tilde{\gamma}^2 k s (1 - s) = \gamma^2 s (1 - s) / k \quad (5)$$

This implies that fluctuations of the input –as measured by the standard deviation σ_s – are proportional to $1/\sqrt{k}$, as expected from the central limit theorem [2, 3]. Also, it follows that the states ($s = 0$ and $s = 1$) exhibit no fluctuations, and that the maximum level of fluctuations occurs at $s = 1/2$, which coincides with the value of the activity at the critical point γ_c .

Moreover, we assumed that each node has k inbound connections and a fixed number n of inhibitory neighbors, but, as a matter of fact, it is also possible to consider the non-regular network case by letting k to be a random variable itself, distributed according to some arbitrary probability distribution $g(k)$. This generalization changes Eq.(4) to

$$p(\Lambda_{jl}) = \sum_{k=1}^{+\infty} \sum_{n=0}^k \binom{n}{l} \binom{k-n}{j} g(k) \cdot h(n|k) s^{j+l} (1-s)^{k-j-l} \quad (6)$$

where $h(n|k)$ is the probability of having n inhibitory neighbors, given a connectivity k . Although the sum cannot be worked out analytically, it is still possible to work it out numerically. In particular, letting $g(k)$ to be a Poisson distribution and $h(n|k)$ a binomial distribution with probability α , it is possible to obtain results for Erdős-Rényi networks.

4 Derivation of the critical and saturation points

Considering the distribution of possible inputs for each node in the annealed approximation, it is straightforward to derive the critical and saturation points of the system. The equation for the activity reads $\dot{s} = \langle f(\Lambda) \rangle - s$. Given Eq.(4) it is possible to compute exactly the average value $\langle f(\Lambda) \rangle$:

$$\langle f(\Lambda) \rangle = \sum_{j=0}^{k-n} \sum_{l=0}^n f(\tilde{\gamma}(j-l)) p_{lj}(s), \quad (7)$$

where n is the number of inhibitory neighbors of a node, and j and l represent the number of active excitatory and inhibitory neighbors, respectively. Although for the hyper-regular case $n = k\alpha$, we consider here a generic n value and replace it by its value at the end of the calculation. Due to the non-linearity of the function f , it is not possible to fully solve the problem analytically. However, it is still possible to derive relevant information from equation (7). First of all, near the critical point γ_c^e , one expects to have a very low level of activity, which suggests to expand Eq.(7) up to first order in s . The probability $p_{lj}(s)$ contains a factor $s^{j+l}(1-s)^{k-j-l}$, so that, if k is large enough (and taking into account that for $\alpha = 0.2$ we should assume $k > 5$ here), all terms with $j+l \geq 2$ contribute to second order in s . Thus, the (j, l) pairs that contribute to first order are just $(0, 0)$, $(0, 1)$ and $(1, 0)$. Of these terms, note that $f(\Lambda_{00}) = f(\Lambda_{01}) = 0$, so, the only contributing one is $(1, 0)$. Taking this value in Eq.(7) and performing the Taylor expansion, one readily obtains

$$\begin{aligned} \langle f(\Lambda) \rangle &= f(\tilde{\gamma}) \binom{n}{0} \binom{k-n}{1} s (1-s)^{k-1} \simeq \\ &\simeq f(\tilde{\gamma}) k (1-\alpha) s. \end{aligned} \quad (8)$$

Considering also that $f(\tilde{\gamma}) = \tilde{\gamma}$, we obtain

$$\dot{s} = \gamma(1-\alpha)s - s, \quad (9)$$

that exhibits a bifurcation at $\gamma_c^e = 1/(1-\alpha)$ separating the quiescent phase ($s = 0$) from the LAI phase ($s \neq 0$).

In order to obtain information about the saturation of the activity one can use the very same procedure to expand around $s = 1$. Observe that now the three pairs that contribute to

first order in $(1 - s)$ are $(k - n, n)$, $(k - n - 1, n)$ and $(k - n, n - 1)$, and $f(\Lambda_{ji})$ does not vanish for any of these terms. Introduce such values in Eq.(7), and after Taylor expanding, one finds:

$$\begin{aligned} \langle f(\Lambda) \rangle &= f[\tilde{\gamma}(k - 2n)] [1 + k(1 - s)] + \\ &+ (1 - s)(k - n)f[\tilde{\gamma}(k - 2n - 1)] + \\ &+ nf[\tilde{\gamma}(k - 2n + 1)]. \end{aligned} \quad (10)$$

To short the notation, we define

$$\begin{aligned} f(\Lambda_0) &\equiv f[\tilde{\gamma}(k - 2n)] [1 + k(1 - s)], \\ f(\Lambda_-) &\equiv f[\tilde{\gamma}(k - 2n - 1)], \\ f(\Lambda_+) &\equiv f[\tilde{\gamma}(k - 2n + 1)], \end{aligned}$$

where all Λ implicitly depend on γ . Thus, depending on the value of the synaptic strength, some the above terms can saturate, i.e. $f(\Lambda) = 1$. In fact, if we that $\gamma > \gamma_c$, then $f(\Lambda_+) = f(\Lambda_0) = 1$. Under this assumption, replacing the value at which the bifurcation happens in Eq.(1), we obtain

$$\gamma^{sat} = \frac{1 - k(1 - \alpha)}{(1 - \alpha) - k(1 - \alpha)(1 - 2\alpha)}, \quad (11)$$

which coincides very accurately with the point at which the activity becomes $s = 1$ in the sparse model, as observed in numerical simulations (see Fig.S3). Note that at the limit $k \rightarrow +\infty$ this coincides with the mean-field critical point, but for sparse networks, saturation occurs after γ_c . Note that the mean-field can be recovered again if we let all the three functions to be $f(\Lambda) = \Lambda$, i.e. none of them saturates.

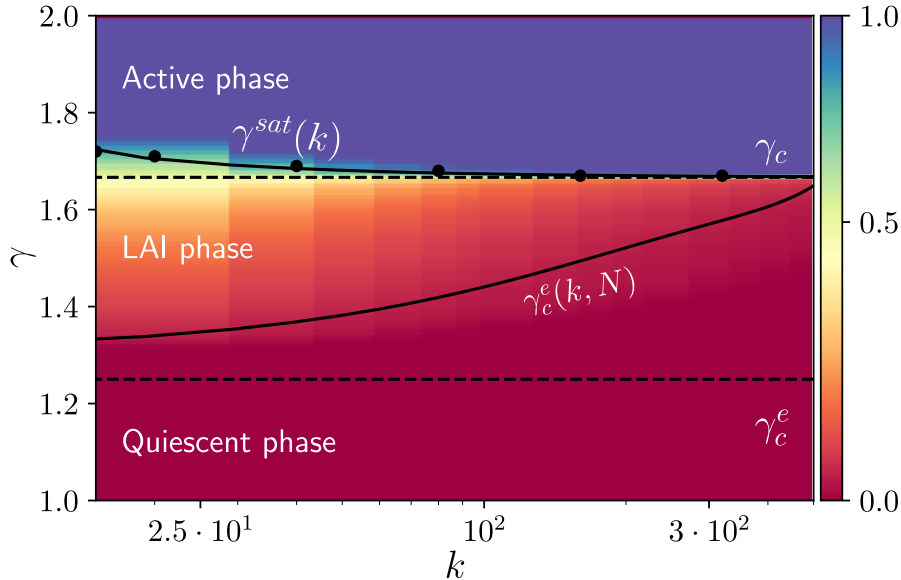


Figure S3: Phase diagram as a function coupling-strength (γ) and connectivity k for a finite size $N = 16000$ nodes; color code indicates the level of averaged overall activity s . This shifts from the quiescent phase (reddish colors) to the active phase (blueish colors). Horizontal dashed lines correspond to the critical points γ_c^e and γ_c at the large- N (thermodynamic) limit. The saturation value $\gamma^{sat}(k)$ corresponds to Eq.(11); results from simulation are marked as black points. The curve $\gamma_c^e(k, N)$ represents an interpolation of the values obtained from simulations, coincides with the dashed line in the large- N limit.

5 Robustness of the results

Here we explore the robustness of the results and conclusions presented in the main text with respect to the modification of various modelling choices.

Changes in the transfer function

First we discuss modifications in the transfer function $f(\Lambda)$, that represents the probability of activation of a neuron with input Λ . The characteristics of the mean-field phase transition, depend on the particular election of this function, as discussed in Appendix 2: it can be either continuous, discontinuous, or discontinuous with bistability and hysteresis. For example, if we use $f(\Lambda) = \tanh(\Lambda)$ for $s > 0$ (and $f(s) = 0$ otherwise), the order of the transition changes from first order to second order. We have computationally verified that the presence of the self-sustained LAI phase is not altered by the choice of $f(\Lambda)$; it exists both in the case in which the mean-field transition is continuous (see Fig.S4) and discontinuous with bistability and hysteresis (see Fig.S5).

In particular, we wondered whether the asynchronous irregular spiking and other characteristic features of the LAI phase –as reported in the main text– are exclusive of the LAI phase or also appear in the active phase in the case in which this exhibits a low level of activity (e.g. in the case of a continuous phase transition, such as that of Fig.6 central). Fig.S4) shows the coefficient of variation (CV) and time-lagged cross-correlation (CC), revealing that both of these quantities are approximately constant and large inside the LAI phase, but they decay quickly as soon as the coupling parameter γ enters the active phase. We conclude that the dynamical properties of the characteristic features of the LAI phase cannot be found in a regular active phase, even when this also displays relatively low activity.

In the case of the continuous mean-field transition, we can take advantage of the functional form of the hyperbolic tangent, in order to compute analytically an expression for the Jensen's force. If the response function $f(\Lambda)$ can be expanded in Taylor series (for $s > 0$), we can approximate the Jensen's stochastic force as

$$F(\Lambda) = \sum_{n=0}^{+\infty} \frac{f^{(n)}(0)}{n!} (\langle \Lambda^n \rangle - \langle \Lambda \rangle^n), \quad (12)$$

for positive inputs. The moments of the input distribution may be computed as shown in the previous Appendix, and thus it is possible to obtain an analytic approximation to the desired order n . If we use $f(\Lambda \geq 0) = \tanh \Lambda$, performing the expansion¹ we obtain that the first term that contributes to the Jensen's force is the one that corresponds to the third moment,

$$F(\Lambda) \equiv F(s) \simeq \frac{\gamma^3}{3} \alpha(1-\alpha)(1-2\alpha)ks(1-s)(1-2s). \quad (13)$$

Observe that in this case the Jensen's force vanishes at $s = 0, 1/2, 1$, in agreement with what we noticed numerically in the main text for the case of the linear piecewise function. In particular, let us also remark that –in the detailed-balanced case– where the mean-field term vanishes and the dynamics is given $\dot{s} = F(s)$, $F(s)$ is of the form ² $F(s) \sim as - bs^2$, showing the continuous quiescent-active transition.

¹Since we use $f(\Lambda < 0) = 0$, the response function is not analytic at the origin –hence, it cannot be Taylor expanded at 0. However, we assume that the expansion is formally valid for all $\Lambda > 0$. A similar calculation cannot be performed for the linear piecewise function, due to the saturation condition $f(\Lambda \geq 1) = 1$.

²Since $0 \leq s \leq 1$, the $+cs^3$ does not destabilize the system, and can be ignored.

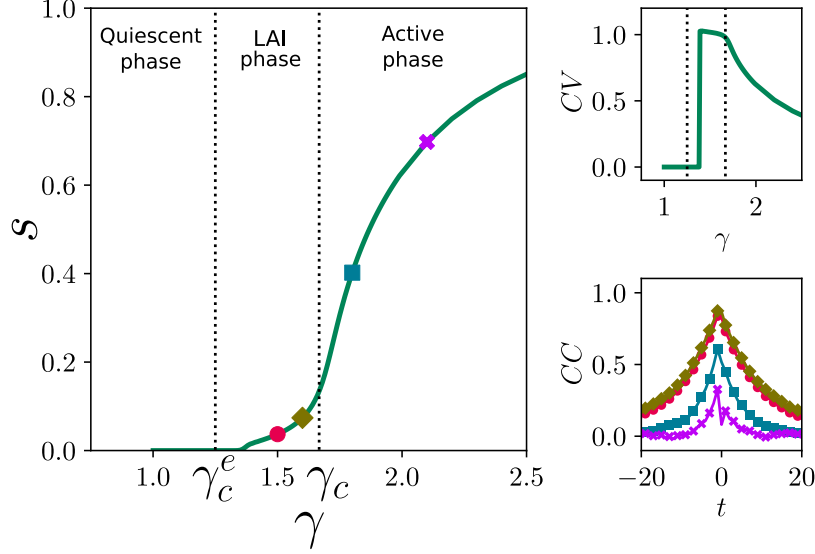


Figure S4: (a) Phase diagram for a model using a hyperbolic tangent (for $s > 0$ and 0 otherwise) as a transfer function in a hyper-regular network with $N = 16000$ nodes and $k = 40$. The critical points, γ_c^e and γ_c , are marked with dotted lines. Observe the presence of an intermediate (LAI) phase, as well as an active phase that emerges after a second-order, continuous phase transition. (b) Coefficient of variation as a function of the coupling γ . Note that CV is approximately constant inside the LAI phase, where it takes a large value. The value of the CV , however, decreases as soon as one enters the active phase. (c) Time-lagged cross-correlations CC for the points marked with symbols in the panel (a). Again, as one goes inside the active phase, the maximum of the correlation starts decreasing, meaning that excitation and inhibition become progressively decorrelated within the active phase.

In the case in which the mean-field phase transition is discontinuous with bistability and hysteresis (see Appendix 2), it is also pertinent to ask whether the emerging LAI phase is able to coexist with the active phase. In order to do that, we consider $f(\Lambda) = \Lambda + \Lambda^3 - c\Lambda^5$ and run simulations for different initial activities s_0 ³. Results are presented in Fig.S5: there is coexistence between the LAI phase (with low but non-vanishing activity) and the active phase. Low initial activity values end up flowing to the LAI state, while higher values of s_0 drive the system to the active phase, with larger values of the activity, illustrating the bistability of the dynamics. When γ is increased, s slowly increases, until the activity value goes over the instability point (smaller than the mean-field value $\gamma_c = 1/(1 - 2\alpha) = 1.667$). Above this point, the LAI phase becomes unstable and the system jumps into the active phase. Thus the system exhibits bistability and hysteresis, between the LAI phase and the regular active one.

³This transfer function is similar to the truncated Taylor expansion of the hyperbolic tangent, changing signs of the non-linear term coefficients. The c term controls the width of the hysteresis cycle, and has been set to $c = 1/2$.

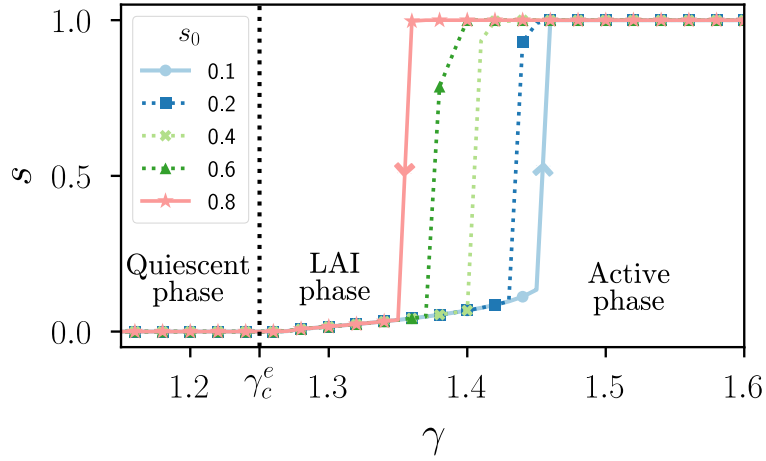


Figure S5: Phase diagram for a transfer function $f(\Lambda) = \Lambda + \Lambda^3 - \frac{1}{2}\Lambda^5$, for different initial states s_0 (see legend). The system displays bistability between the LAI phase and the active phase in a full interval of γ values. $N = 128000$ and $k = 15$.

Changes in the network structure

Simulations for annealed and quenched hyper-regular networks show that both cases give the same results computationally, and that such results coincide with the analytic predictions. Thus, as analytical computations are exact only in the annealed case, the essence of the involved mechanism has nothing to do with the network specific structure and, thus, spectral analyses of the connectivity matrix [4, 1] do not add much to the understanding of the noise-induced intermediate phase.

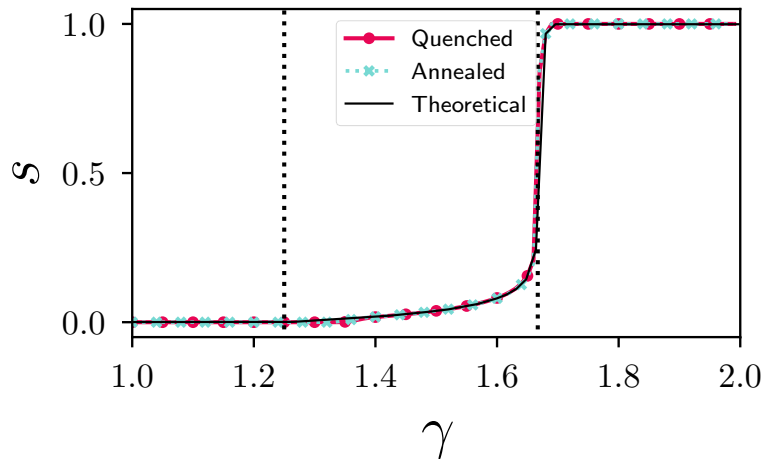


Figure S6: Comparison between annealed and quenched networks (simulation results marked with symbols) and the theoretical prediction for hyper-regular networks with connectivity $k = 40$ and size $N = 16000$. The agreement between quenched and annealed hyper-regular networks is excellent (perfect within numerical accuracy), and the agreement between these two and analytical predictions is also excellent for sufficiently large network sizes.

We verified computationally that the main results also emerge in more irregular networks. In particular, simulations on Erdős-Rényi networks also reveal the emergence of a LAI phase, as shown in Fig.S7. Similarly, considering a Gaussian distribution of weights with variance $\sigma^2 = 1$ (rather than ± 1), does not affect either the existence of a LAI phase (see Fig.S7).

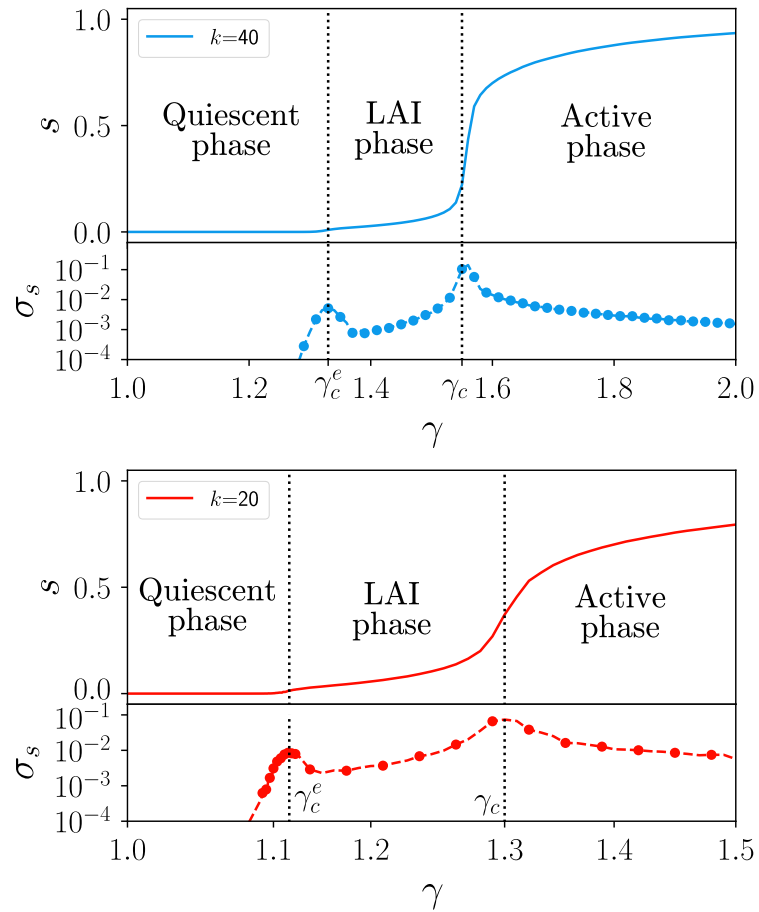


Figure S7: (Up) The LAI phase emerges also in (non-regular) unweighted Erdős-Rényi networks with mean connectivity $k = 40$ and $N = 16000$ as well as in (Down) Erdős-Rényi networks with a Gaussian weight distribution, $k = 20$ and $N = 16000$.

6 Avalanches at criticality

Here we scrutinize the dynamics at the noise-induced critical point, separating the quiescent from the LAI phase. In particular, we analyze the emergence of avalanches of activity originated after introducing a seed of activity into an otherwise quiescent state. We observed computationally that at the quiescent-active critical point γ_c^e the system displays avalanches –whose sizes and durations are distributed as power-laws as $P(S) \sim S^{-\tau}$ and $P(T) \sim T^{-\alpha}$, respectively– thus compatible with those of the unbiased branching process (see Fig.S8).

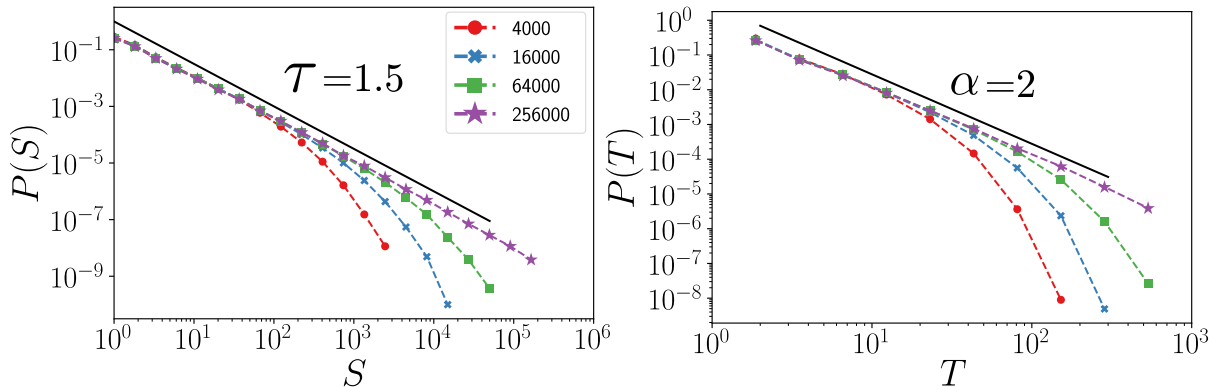


Figure S8: Distribution of avalanche sizes (left) and durations (right) at the critical point γ_c^e for different system sizes (see legend) in a hyper-regular network with $k = 15$. Black dotted lines are guides to the eye showing the theoretical values for the unbiased branching process.

On the other hand, at the second critical point, γ_c –separating the LAI from the active phase– there are not scale-free avalanches, but just excursions of the global activity around its mean value (results not shown).

7 Damage spreading in the asynchronous state

As shown in Fig.S9a, all across the LAI phase we observe a value of $B > 1$, and, as a consequence, chaotic behavior, as previously suggested for asynchronous states [2]. Moreover, as shown in Fig.S9b, flipping a small number of nodes (e.g. 10 nodes) the networks fulfill completely different dynamical states in the LAI phase. Thus, by computing the difference between states in M and M' , averaged in time for sufficiently large times (H_{st}), one observes that –within the LAI phase– this difference takes almost the same value as the network activity, revealing that the active sites become rapidly uncorrelated in both replicas, reflecting again the chaotic nature of the LAI phase.

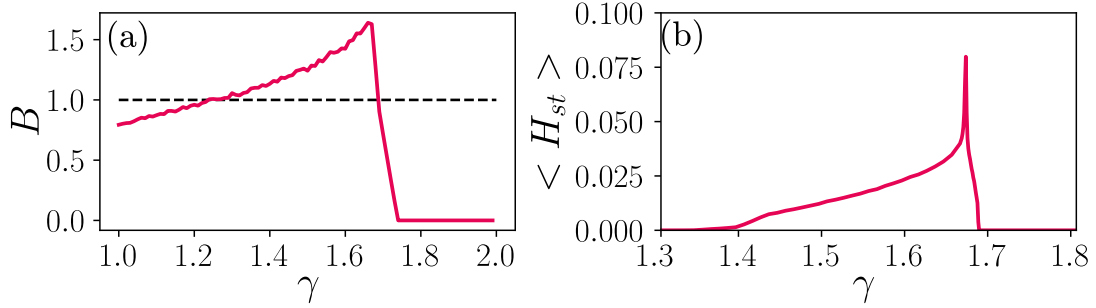


Figure S9: (a) Branching function B in damage spreading experiments (averaged over 10^4 runs). Black dotted lines represent marginal propagation of activity, i.e. critical dynamics. All across the LAI phase, the dynamics propagates in a chaotic way $B > 1$, while in the quiescent and active phases, the Hamming distance is smaller than 1. (b) Average over runs for the time-averaged Hamming distance in the steady state $\langle H_{st} \rangle$, over $T = 10^4$ MonteCarlo steps; the two initial replicas are different in a small number (10) of nodes. In this case, within the LAI phase the difference between the two replicas $\langle H_{st} \rangle$ is very close to the steady state density, indicating that activity becomes uncorrelated between them (node states coincide only by chance). Simulations run for hyper-regular networks with $N = 16000$, $k = 40$ and $\alpha = 0.2$.

8 Experimental measurement of Jensen's force

In order to explicitly observe and measure Jensen's forces in the laboratory, we propose the following (preliminary) experimental protocol:

(i) Consider observations of neuronal activity in the asynchronous state such as those already in the existing literature. Measure the average network activity $s(t)$ as a function of time (in discrete time bins) and determine the value $s(t+1)$ as a function of the activity at the preceding timestep $s = s(t)$ for all possible observed values of s and average across the steady-state time series to obtain good statistics. This procedure provides us with an empirical estimation of the averaged response transfer function as $s(t+1) = \langle f(\Lambda) \rangle_{exp}$ (as easily derived from Eq.(??)). Let us remark that there exist publicly available empirical datasets (e.g. for the rat and cat cortex; see [5] and refs. therein) that can be used for this purpose, though better statistics including many more neurons and longer observations times would be highly desirable.

(ii) Extract individual neurons from the same tissue under study and determine empirically *in vitro* their associated transfer function $f_{exp}(\Lambda)$ (where Λ is the input). We believe that this is experimentally feasible as similar measurements have been already successfully performed [6, 7]. If, in the experiments, the responses of diverse neurons are different, a sort of averaged neuron response should be constructed as a proxy for $f_{exp}(\Lambda)$ [6].

(iii) Measuring the membrane potential, it should be possible to estimate the averaged input received by a single neuron in the network, $\langle \Lambda \rangle$ and using the result of (ii) it should be possible to compute $f_{exp}(\langle \Lambda \rangle)$.

(iv) The state-dependent Jensen's force is then determined using Eq.(??), i.e.

$$F(\Lambda) = \langle f(\Lambda) \rangle_{exp} - f_{exp}(\langle \Lambda \rangle). \quad (14)$$

The theory presented here predicts a non-linear and non-monotonic behavior for $F(\Lambda)$, similar to that of the inset of Fig.3. Note also that the theoretical prediction could be refined and made more specific by implementing in the theoretical model the empirically determined transfer function, $f_{exp}(\Lambda)$. This change might hinder analytical calculations, but would be straightforward to implement in computational analyses of our simple model, that would lead to a specific prediction for the Jensen's force in the experimental setup. In any case, for states

of low activity the difference between the averaged response within the network $\langle f_{exp}(\Lambda) \rangle$ is expected –according to the theory developed here– to be larger than the response of individual neurons to the average activity $f_{exp}(\langle \Lambda \rangle)$, i.e. there should be a repulsive stochastic force, inducing fluctuating states of low-activity, and this should be observed in the experiments.

We leave this programme –which is very likely to need refinements to account for a number of potential experimental pitfalls, such as statistical error from subsampling, time-binning ambiguities, heterogeneous response of individual neurons, etc.– for future research and as an open challenge for experimentalists.

References

- [1] Binney, J. J., Dowrick, N. J., Fisher, A. & Newman, M. E. *The Theory of Critical Phenomena* (Oxford University Press, Oxford, 1993).
- [2] Van Vreeswijk, C. & Sompolinsky, H. Chaos in neuronal networks with balanced excitatory and inhibitory activity. *Science* **274**, 1724–1726 (1996).
- [3] Barral, J. & Reyes, A. D. Synaptic scaling rule preserves excitatory–inhibitory balance and salient neuronal network dynamics. *Nat. Neurosci.* **19**, 1690 (2016).
- [4] Chen, X. & Dzakpasu, R. Observed network dynamics from altering the balance between excitatory and inhibitory neurons in cultured networks. *Phys. Rev. E* **82**, 031907 (2010).
- [5] Zierenberg, J., Wilting, J. & Priesemann, V. Homeostatic plasticity and external input shape neural network dynamics. *Phys. Rev. X* **8**, 031018 (2018).
- [6] Wolfart, J., Debay, D., Le Masson, G., Destexhe, A. & Bal, T. Synaptic background activity controls spike transfer from thalamus to cortex. *Nat. Neurosci.* **8**, 1760 (2005).
- [7] La Camera, G. *et al.* Multiple time scales of temporal response in pyramidal and fast spiking cortical neurons. *J. Neurophysiol.* **96**, 3448–3464 (2006).